Acta Pharmaceutica Sinica B 2023;13(12):5091−5106

Chinese Pharmaceutical Association
Institute of Materia Medica, Chinese Academy of Medical Sciences

Acta Pharmaceutica Sinica B

www.elsevier.com/locate/apsb
www.sciencedirect.com

ORIGINAL ARTICLE

# An injectable signal-amplifying device elicits a specific immune response against malignant glioblastoma

**Qiujun Qiu[a], Sunhui Chen[b], Huining He[d], Jixiang Chen[a], Xinyi Ding[a], Dongdong Wang[a], Jiangang Yang[a], Pengcheng Guo[a], Yang Li[a], Jisu Kim[a], Jianyong Sheng[a], Chao Gao[a,f], Bo Yin[e], Shihao Zheng[g], Jianxin Wang[a,c,*]**

[a]*Department of Pharmaceutics, School of Pharmacy, Fudan University & Key Laboratory of Smart Drug Delivery, Ministry of Education, Shanghai 201203, China*
[b]*Department of Pharmacy, Fujian Provincial Hospital & Provincial Clinical Medical College of Fujian Medical University, Fuzhou 350001, China*
[c]*Institute of Materia Medica, Academy of Chinese and Western Integrative Medicine, Fudan University, Shanghai 201203, China*
[d]*Tianjin Key Laboratory on Technologies Enabling Development of Clinical Therapeutics and Diagnostics, School of Pharmacy, Tianjin Medical University, Tianjin 300070, China*
[e]*Department of Radiology, Huashan Hospital, Fudan University, Shanghai 200040, China*
[f]*Institute of Tropical Medicine, Guangzhou University of Chinese Medicine, Guangzhou 510006, China*
[g]*Department of Neurosurgery, Fujian Provincial Hospital & Provincial Clinical Medical College of Fujian Medical University, Fuzhou 350001, China*

Received 15 March 2023; received in revised form 4 June 2023; accepted 5 June 2023

**KEY WORDS**

Immunotherapy;
Glioblastoma;
Antigen-capturing nanoparticles;
Recombinant chemokines;
Immune signal-amplifying

**Abstract** Despite exciting achievements with some malignancies, immunotherapy for hypoimmunogenic cancers, especially glioblastoma (GBM), remains a formidable clinical challenge. Poor immunogenicity and deficient immune infiltrates are two major limitations to an effective cancer-specific immune response. Herein, we propose that an injectable signal-amplifying nanocomposite/hydrogel system consisting of granulocyte-macrophage colony-stimulating factor and imiquimod-loaded antigen-capturing nanoparticles can simultaneously amplify the chemotactic signal of antigen-presenting cells and the "danger" signal of GBM. We demonstrated the feasibility of this strategy in two scenarios of GBM. In

*Corresponding author.
E-mail address: jxwang@fudan.edu.cn (Jianxin Wang).

Peer review under responsibility of Chinese Pharmaceutical Association and Institute of Materia Medica, Chinese Academy of Medical Sciences.

https://doi.org/10.1016/j.apsb.2023.06.010

system;
Postoperative relapse;
Biomaterial;
Vaccine

the first scenario, we showed that this simultaneous amplification system, in conjunction with local chemotherapy, enhanced both the immunogenicity and immune infiltrates in a recurrent GBM model; thus, ultimately making a cold GBM hot and suppressing postoperative relapse. Encouraged by excellent efficacy, we further exploited this signal-amplifying system to improve the efficiency of vaccine lysate in the treatment of refractory multiple GBM, a disease with limited clinical treatment options. In general, this biomaterial-based immune signal amplification system represents a unique approach to restore GBM-specific immunity and may provide a beneficial preliminary treatment for other clinically refractory malignancies.



## 1. Introduction

Immunotherapy for various hypoimmunogenic cancers presents a formidable clinical challenge, especially for glioblastoma (GBM), the most aggressive and immunoevasive tumour occurring in the central nervous system (CNS); GBM currently has an extremely poor prognosis and no curative treatment options[1]. Surgical resection is the primary approach to excise the tumour bulk, however, tumour recurrence is inevitable after surgery[2–4]. Immunotherapies with mild toxicity and durable responses have changed the treatment landscape of various malignancies[5–7] but not that of GBM[8], which can be attributed to poor immunogenicity and inadequate immune infiltrates in that area of the body[7,9].

The CNS parenchyma has historically been recognized as being immune privileged (Fig. 1A). The absence of lymphatic drainage accompanied by the paucity of antigen-presenting cells (APCs) poses the greatest challenge for GBM immunotherapy[7,10]. However, the discovery of functional lymphatic vessels in the meninges refutes this classic dogma and provides a pathway for antigen drainage from the brain and APCs entry into peripheral lymph nodes[11,12]. Produced in the bone marrow and attracted to the central lesion during the disease process, dendritic cells (DCs) are the most potent APCs and play a key role in the initiation of anti-GBM immune responses[13]. Granulocyte-macrophage colony-stimulating factor (GM-CSF) is one of the most important factors in the recruitment and proliferation of DCs. Porous biomaterial scaffolds loaded with GM-CSF have proven to be a promising strategy to increase the chemotactic signal and replenish DCs against multiple tumours and could have an effect on GBM[14–16]. However, classified as a cold tumour immune milieu, GBM is poorly immunogenic and prone to immune escape[17,18], which is another cause of immunotherapy failure. Systemic therapeutic strategies, including immune checkpoint inhibition and combination chemotherapy, have been attempted to treat GBM by externally boosting the immune response, but limited intracerebral penetration (ordinarily under 1% of the total dose)[19–21] leads to severe off-target effects and myelosuppression[22,23], which in turn counteracts the outcome of the immunotherapy.

To alleviate these two major obstacles, we propose an injectable nanocomposite/hydrogel system (DOX/RAcNPs@GM gel) consisting of doxorubicin (DOX), granulocyte-macrophage colony-stimulating factor (GM-CSF) and imiquimod-loaded antigen-capturing nanoparticles (RAcNPs) to simultaneously amplify the chemotactic signal of antigen-presenting cells and the "danger" signal of GBM antigens (Fig. 1B). Surgical debulking is the first clinical intervention for GBM patients[24], resulting in a cavity for therapeutic implantation to circumvent both the blood–brain barrier and systemic side effects[25]. Early recurrence of GBM normally occurs near the resection site; thus, the fast release of the chemotherapeutic agent DOX after implantation inhibits early recurrence and facilitates tumour-associated antigen (TAA) exposure. Additionally, RAcNPs can efficiently capture TAAs released from moribund cells through non-covalent hydrophobic–hydrophobic interactions[26], subsequently facilitating the cytosolic delivery of these antigen proteins to maximize the amplification of the immunogenic signals of GBM. Moreover, the gradual release of GM-CSF amplifies the chemotactic signal and ceaselessly enriches DCs to counteract the low infiltration of APCs, ultimately turning a cold GBM hot and suppressing late recurrence (Fig. 1C).

In the second phase of our study, we further propose an immune-amplifying hydrogel as a safe and effective vaccine by extracranially enriching, reprogramming, activating, and releasing DCs (Fig. 8A). We hypothesize that encapsulation of the TOLL-like receptor (TLR) 7 agonist R837 in nanoparticles may construct a nano-vaccine capable of co-delivering tumour antigens and adjuvants, which synergistically amplify the immune signals with the GM-CSF hydrogel to inhibit the growth of unresectable multiple GBM.

## 2. Materials and methods

### 2.1. Patient MRI images

Patient magnetic resonance imaging (MRI) images were obtained from the Department of Neurosurgery, Fujian Provincial Hospital, Fuzhou, China. All the patient information was obtained with written informed consent and collected using a standard protocol approved under the Review Board of Fujian Provincial Hospital (Application No. K2022-04-010).

### 2.2. Materials, cell lines, and animals

DOX hydrochloride, R837, poly(lactic-co-glycolic acid) ($PLGA_{75/25}$) and 1,1′-dioctadecyl-3,3,3′,3′-tetramethylindodicarbocyanine perchlorate (DiD) were obtained from Meilunbio (Dalian, China). Medical-grade sodium alginate was purchased from Shanghai Aladdin Biochemical Technology Co., Ltd. (Shanghai, China). DSPE-PEG was purchased from Shanghai Advanced Vehicle Technology Co., Ltd. (Shanghai, China). GM-CSF was purchased from PeproTech

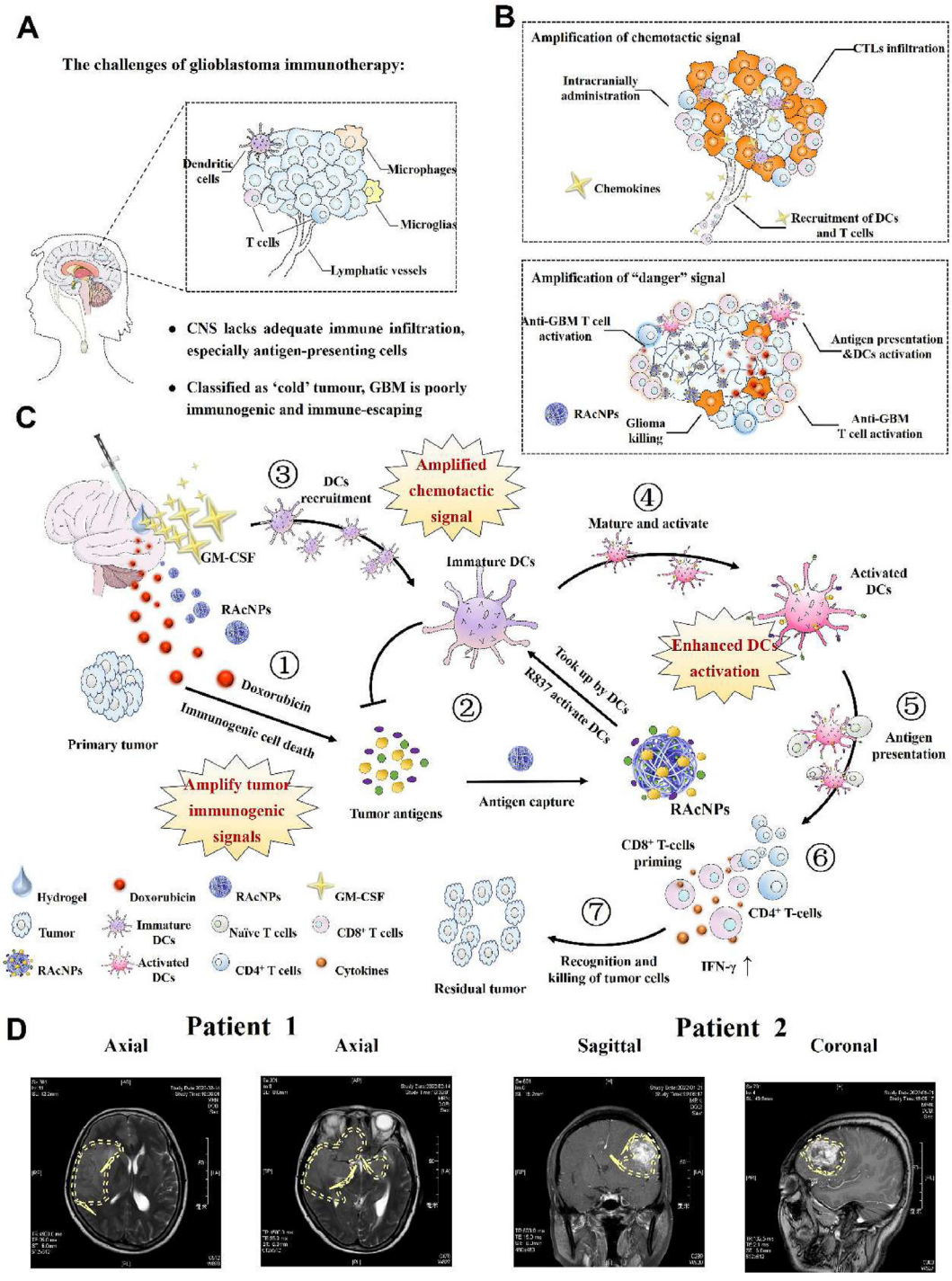


**Figure 1** Scheme of DOX/RAcNPs@GM gel for suppression of postoperative glioblastoma (GBM) recurrence. (A) The challenges of GBM immunotherapy. (B) Sequential release of granulocyte-macrophage colony-stimulating factor (GM-CSF) and imiquimod-loaded antigen-capturing nanoparticles (RAcNPs) for the amplification of chemotactic and "danger" immune signals. (C) Scheme for the synergistic amplification of GBM immune signalling by DOX, GM-CSF, and RAcNPs. 1) The release of DOX induces tumour ICD and tumour-associated antigen (TAA) exposure; 2) R837-loaded NPs capture TAAs and facilitate the cytosolic delivery; 3) GM-CSF ceaselessly attracts and enriches dendritic cells (DCs) in GBM; 4) reprogramming and activation of DCs; 5) antigen cross-presentation; 6) T lymphocyte expansion; 7) killing of residual GBM cells by activated T cells. (D) Magnetic resonance images of patients with intracranial GBM. The yellow line depicts the indistinct and irregular border between the GBM and normal brain tissue.

(USA). Surgical instruments for GBM resection were purchased from Shenzhen Reward Life Technology Co., Ltd. (Shenzhen, China) and pre-sterilized by autoclaving before surgery.

Murine GBM cells C6 and GL261 and human GBM cells U87 were cultured in DMEM medium (BasalMedia, Shanghai, China), supplemented with 10% fetal bovine serum (FBS), 100 U/mL penicillin and 100 μg/mL streptomycin. DC2.4 cells were cultured in RPMI 1640 medium (BasalMedia, Shanghai, China) containing the same concentration of FBS and antibiotics. Cells were cultured at 37 °C in a humidified atmosphere with 5% $CO_2$ before the test.

Male BALB/c and C57 mice and male SD rats at 6−8 weeks were obtained from Shanghai SLAC Laboratory Animal Co., Ltd. and housed under specific-pathogen free conditions. All the animal protocols were approved by the Institutional Animal Care and Use Committee of Fudan University. Animals were allowed to eat freely and randomized before the experiment.

### 2.3. Fabrication and characterization of DOX/RAcNPs@GM gel

RAcNPs were prepared by the emulsification-diffusion method[27,28]. Briefly, 10 mg $PLGA_{75/25}$ (MW = 30 kDa) were first dissolved in dichloromethane. 4 mg/mL R837 DMSO solution was added dropwise at a ratio of PLGA: R837 = 20:1. Subsequently, 2 mL polyvinyl alcohol (PVA, 5%, *w/v*) solution was added and shaken repeatedly to fully blend. The mixture was ultrasonicated at a power of 400 W for 12 min. The suspension was supplemented with another 2 mL 5% PVA solution and stirred under magnetic for 4 h. After stirring, the organic solvent was removed by vacuum rotary evaporation. RAcNPs were subsequently filtered through a sterile filter, centrifuged at 15,000 rpm for 30 min (SCILOGEX, CF1524R, Houston, USA), and washed twice with PBS. The PEG-modified nanoparticles (PEG-NPs) were prepared in the same method, except that 3.33 mg of PEG-PLGA conjugate was additionally added to the dichloromethane solution. The size, zeta potential, and PDI of various NPs were measured using a Malvern Zetasizer Nano ZS90 (Malvern Instruments Ltd., UK) and the NPs morphology was observed using a TEM (FEI Tecnai G2 Spirit 120 Kv, USA). Also, the particle size and PDI of the nanoparticles were measured at different days to determine the long-term stability.

The pharmaceutical-grade ALN powder was added to an appropriate amount of redistilled water and soaked overnight, and then stirred at 60 °C in a water bath to dissolve completely. Concentrated DOX and GM-CSF solution was formulated and sterilized through sterile filters. To fabricate the DOX/RAcNPs@GM gel, sterilized DOX, GM-CSF, as well as RAcNPs were mixed with ALN hydrogel at 4 °C for 0.5 h, and double-distilled water was finally added to adjust the ALN concentration to 1.5% (*w/v*). Vials and stir bars for the hydrogel preparation were autoclaved before use. The morphology of ALN hydrogel was imaged using a field SEM (FEI Nova NanoSEM 450, USA). Hemolytic tests of DOX, RAcNPs, and GM-CSF hydrogel were performed. The release of DOX, R837, and GM-CSF in ALN hydrogel was studied with continuous shaking at 37 °C. On Days 0.25, 0.5, 1, 2, 4, 6, 8, 10, 12, 14, and 16, the solution was sampled and replenished with fresh medium. Released DOX and RAcNPs were determined using a microplate reader (Bio-Tek, USA) and the released GM-CSF was measured using a GM-CSF kit. In addition, the ALN hydrogel were weighed on different days to determine the *in vitro* degradation.

### 2.4. Cytotoxicity analysis

Cytotoxicity analysis of DOX was performed on murine GBM cells C6 and GL261 and human GBM cells U87. In brief, cells were plated in a 96-well plate at $5 \times 10^3$ cells/well. After a 24 h culture, the medium is discarded and replaced with 100 μL fresh medium containing DOX at concentrations ranging from 0.04 to 25 μmol/L. Cells were incubated at 37 °C in a 5% $CO_2$ atmosphere for 24 or 48 h. After incubation, 25 μL MTT reagent (2 mg/mL) was added to each well and the plate was incubated for an additional 4 h. After removal of the medium, 150 μL of DMSO was added to each well to dissolve the formazan crystals and the absorbance at 570 nm was measured using a microplate reader (Bio-Tek, USA). For determining the cytotoxicity of DOX on U87 cells, cells were treated with DOX in the same procedure. After incubation, 10 μL CCK-8 was added to each well and incubated for another 3.5 h and the absorbance was measured at 490 nm. GBM cells without DOX treatment served as a positive control. Cell viability was calculated by the following Eq. (1):

$$\text{Cell viability } (\%) = (OD_{test} - OD_{background}) / (OD_{untreatment} - OD_{background}) \times 100 \quad (1)$$

### 2.5. TAAs exposure, capture, and cytosolic delivery

Murine GBM cells C6 and GL261 and human GBM cells U87 were first seeded in a 24-well plate ($1 \times 10^5$ per well) overnight. After washing with PBS, cells were treated with a serum-free medium containing various concentrations of DOX (0, 1, 5, 10 μg/mL) for 12 h. The supernatant was collected and spun down at 5000 rpm for 20 min (SCILOGEX) to remove insoluble cellular debris. Afterward, TAAs were collected and the HMGB1 protein was determined by HMGB-1 ELISA Kit (Shanghai Jingkang bio, China), according to the manufacturer protocols. For the visualization of ICD markers, C6, Gl261 and U87 cells pre-treated with 10 μg/mL DOX were incubated with CRT antibody (Novus Biologicals, USA) for 0.5 h at room temperature. After washing with PBS, cells were fixed with 4% paraformaldehyde, counterstained with DAPI (Meilunbio, China), and finally visualized with CLSM.

To determine the TAAs captured by NPs, 2 mg of each NPs was mixed with 1 mg antigens from ten million cells and stirred for 2 h. Subsequently, the NPs were centrifuged at 15,000 rpm for 30 min (SCILOGEX) to remove the unadsorbed protein. The amount of antigen bound by the RAcNPs or non-R837-loaded nanoparticles (AcNPs) was determined using a bicinchoninic acid analysis.

To demonstrate the enhanced intracellular delivery of TAAs by NPs, TAAs were collected and subsequently incubated with RAcNPs or PEG-NPs at 4 °C for 2 h with agitation. Hereafter, TAAs complexes were centrifuged at 15,000 rpm for 30 min (SCILOGEX) to remove the unadsorbed protein. Immature DC cells ($1 \times 10^6$ per well) were seeded in a 12-well plate and incubated with TAAs mixture pre-treated with different nanoformulations. After washing with PBS, cells were digested, centrifuged (SCILOGEX), fixed, and finally analyzed by flow cytometry or imaged by CLSM. Antigen/nanoparticle double-positive cells were distinguished by flow cytometry. Free TAAs supernatant without being captured by NPs were set as a control group.

### 2.6. In vitro DCs activation

Mouse BMDCs were used to evaluate the *in vitro* activation ability of DOX and RAcNPs. Firstly, bone marrow progenitor cells were harvested from tibias and femurs of 6−8 weeks-old mice to make

a homogeneous suspension. After lysis of red blood cells, cell pellets were re-suspended in a complete RPMI 1640 medium containing 20 ng/mL GM-CSF and 10 ng/mL IL-4 and seeded in a six-well plate. Each plate was supplemented with fresh medium containing GM-CSF and IL-4 every other day. On Day 6, the medium was collected and centrifuged to concentrate the immature BMDCs. The cells were then seeded in a 24-well plate and further incubated with PBS, DOX-pretreated GBM cells supernatant, 5 μg/mL RAcNPs or 5 μg/mL Free R837 for another 18 h. After incubation, BMDCs were collected, washed with PBS, and stained with fluorescent conjugated CD11c, CD80, and CD86 monoclonal antibodies (mab) at room temperature for 0.5 h. Finally, cells were washed, fixed, and analyzed with a flow cytometer.

### 2.7. *Intracranial retention of DOX/RAcNPs@GM gel*

First, mice were anesthetized by intraperitoneal injection of 1% isopentobarbital. Subsequently, a midline incision of the scalp was made with a sterile scalpel and a small hole for injection of the hydrogel was drilled. Various preparations were injected using a microsyringe with the aid of a brain stereotaxic apparatus (Reward, Shenzhen, China). At different time intervals, mice were anesthetized and imaged with an IVIS (PerkinElmer, USA) to determine the retention of RAcNPs. On Day 12, mice were euthanized and brain tissue was dissected for *ex vivo* IVIS imaging. For the detection of DOX retention, mice were euthanized and brain tissue was dissected for IVIS imaging 12 days after injected with different DOX preparations. To determine the GM-CSF retention, mice were euthanized on Days 1 and 3. Brain tissues were dissected and homogenized by a tissue homogenizer. After centrifugation (SCILOGEX), the supernatant was sampled and GM-CSF was determined using a cytokine kit.

### 2.8. *Intracranial DCs recruitment and cytokine analysis*

For the analysis of intracranial DCs recruitment, mice were first anesthetized and craniotomied in a sterile environment as described above. Mice were intracranially administrated with ALN hydrogel with or without 100 μg/kg GM-CSF *via* a brain stereotaxic apparatus. Brain samples were gathered 6 d after hydrogel was injected, paraffin embedded, and sectioned. Slices were incubated overnight with anti-mouse CD11c mab and visualized by a digital slide scanner (VS200, Olympus, Japan).

To evaluate the synergy of GM-CSF hydrogel with DOX/RAcNPs and to elicit anti-tumour immune responses from the inside out, mice were first injected with DOX-induced GBM antigen, RAcNPs with or without GM-CSF hydrogel at a dose of antigens equivalent to $4 \times 10^5$ GBM cells, 1 mg/kg R837 and 100 μg/kg GM-CSF. Mice in the control group were injected with an equal volume of PBS with the same procedure. Eleven days after formulation administration, mice were euthanized. The cerebral hemisphere and spleen were dissected for cytokine analysis and T lymphocyte analysis, respectively. Hemispheres were fully homogenized and the homogenate was further centrifuged (SCILOGEX). The supernatant was collected, and IFN-$\gamma$, IL-6, and IL-12 were assayed with corresponding ELISA kits (MultiScience, Hangzhou, China) according to the manufacturer's instructions. The tissue was fully ground and filtrated through a 70 μm cell filter to remove the tissue remnants. Cell suspensions were concentrated and lysed on ice for 5 min using erythrocyte lysis buffer (Meilunbio, Dalian, China). Sufficient PBS was added to the cell suspension to terminate the lysis. After the nonspecific adhesion adsorption was blocked, cells were then stained with anti-mice CD3, CD4, and CD8 mab at room temperature for 40 min. The cells were finally analyzed by a flow cytometer (Supporting Information Figs. S12 and S13; Beckman, USA).

### 2.9. *Establishment of recurrent orthotopic GBM model*

The primary GBM model was first established. Male rats aged 6−8 weeks were anesthetized and a mid-scalp incision was made to expose the sagittal and coronal sutures. After disinfecting, a cutting circle with a diameter of approximately 5 mm was created by an electric drill at the right posterior side of the bregma. C6 cells ($5 \times 10^5$ cells per mouse) in 5 μL PBS were slowly injected into the cortex at a 3.5 mm depth by a microsyringe. The stereotaxic coordinates of the cell injection were: 2.0 mm posterior to Bregma and 2.0 mm lateral to the sagittal suture. The scalp was sutured and mice were placed on a heating pad until awake.

Fourteen days after GBM implantation, rats were subjected to living imaging and MRI using a 3T General Electric MRI system (General Electric, USA) to assess the location of intracranial tumour. The tumour resection procedure was performed as the previous report under the guidance of a neurosurgeon[29]. All the instruments were pre-sterilized by autoclaving before surgery. First, a small incision was made in the scalp and the dura was excised. The gross tumour mass was subsequently resected using a hand-held aspiration device according to the MRI images. A degradable gelatin sponge was pressed to the wound to prevent massive hemorrhage. The entire procedure was performed on an animal insulation mat at a suitable temperature.

### 2.10. *Therapeutic effect of DOX/RAcNPs@GM gel on recurrent GBM*

To evaluate the effects of DOX/RAcNPs@GM gel on the regrowth of C6 and survival of the rats, the gross tumour mass was resected and the rats were divided into the following groups 14 days after C6 implantation: (A) control group, rats received only intracranial tumour resection without any subsequent treatment; (B) TMZ group, animals received four i.p. injections of 10 mg/kg TMZ on alternate days; (C) DOX/RAcNPs@gel group, rats received one i.c. administration of DOX and RAcNPs; (D) GM@gel group, rats received one i.c. injections of GM@gel at a dose of 20 μg/kg GM-CSF; (E) DOX/RAcNPs@GM gel group, rats received one i.c. administration of DOX/RAcNPs@GM gel at the same dose to elicit an anti-GBM immune response. All rats were housed in standard-specific pathogen-free facilities and treated by the policies and guidelines of the Chinese National Technical Committee for Standardization of Experimental Animals. The 3T MRI system was used to periodically monitor intracranial tumour volume by T2 sequence and the tumour volume was calculated using a manually drawn region of interest.

### 2.11. *Immuno-amplified effect of DOX/RAcNPs@GM gel*

To evaluate the immuno-amplification of DOX/RAcNPs@GM gel on the C6 resection model, rats were sacrificed after different treatments. Brains were collected and the hemispheres were fully homogenized. The homogenate was centrifuged (SCILOGEX) and IFN-$\gamma$, IL-2 and IL-10, and TGF-$\beta$ in the supernatant were assayed with corresponding ELISA kits (MultiScience, Hangzhou, China) according to the manufacturer's instructions. For

immunochemical and immunofluorescence analysis, brain samples were collected, paraffin embedded, and sectioned. Slices were incubated overnight with CD11c, CD4, and CD8 mab and visualized by a digital slide scanner.

### 2.12. Fabrication of NanoVac@GM gel

To prepare antigen-captured NanoVac, GBM cells were first subjected to 5 cycles of rapid freeze in liquid nitrogen, thaw (37 °C) and then centrifuged at 1000 rpm for 5 min. The supernatant containing tumour lysates was collected and incubated with RAcNPs at 4 °C for 2 h. NPs were prefiltered with a sterile filter. To prepare NanoVac@GM gel, aliquots of GM-CSF were dissolved in a sterile 5% trehalose solution and subsequently mixed with NanoVac and ALN hydrogel. An appropriate amount of PBS was added to adjust the final concentration of ALN to 1.5%. The whole process was carried out on a clean bench.

### 2.13. Immunization

Various vaccines (200 μL) were injected subcutaneously in mice at 6−8 weeks *via* a syringe under brief isoflurane anesthesia. The doses for each mouse were antigens equivalent to $5 \times 10^5$ GBM cells, 100 μg R837, and 1.5 μg GM-CSF. Blank hydrogel without antigens, adjuvant, and GM-CSF was used as a negative control.

### 2.14. Therapeutic effects of NanoVac@GM gel

The therapeutic efficacy of NanoVac@GM gel was assessed on a multiple diffuse GBM model. C6 cells ($2.5 \times 10^5$ cells per mouse) were precisely injected into the ventricles of mice. Multiple tumour foci were observed by MRI several days after tumour inoculation. Six to eight weeks old mice were randomly divided into four groups after tumour implantation. All mice received different subcutaneous treatments two times. During the experiment, mice were housed in sterile SPF-grade laboratories maintained at constant temperature and fed ad libitum. The death events of the mice were recorded.

### 2.15. Systemic immune activation of NanoVac@GM gel

Seven days after the immunization, mice blood was withdrawn from the retro-orbital plexus. Blood samples coagulated naturally for 2 h at 4 °C. Hereafter, blood was centrifugated (SCILOGEX) and serum was separated. Serum INF-$\gamma$ and TNF-$\alpha$ were determined at a certain dilution using corresponding ELISA kits (MultiScience, Hangzhou, China). For spleen T lymphocyte expansion analysis, GBM-bearing mice were euthanized after blood collection. Spleens were separated, ground with the rubber end of syringes and filtrated through a 70 μm cell filter to remove the tissue remnants. Cell suspensions were centrifuged (SCILOGEX) and resuspended with erythrocyte lysis buffer (Meilunbio, Dalian, China). After being incubated on ice for 5 min, lysis was terminated by the addition of 5 volumes of pre-chilled PBS. Subsequently, cells were concentrated and incubated with 1% FBS on ice for 30 min to block the nonspecific adhesion adsorption. Cells were then stained with anti-mice CD11c, CD86, CD3, CD4, and CD8 mab at room temperature for 40 min. After multiple washes, cells were collected, fixed, and finally analyzed by a flow cytometer.

### 2.16. Safety evaluation

Acute toxicity experiments were performed on healthy mice at 6−8 weeks. Experimental mice were randomly divided into the following groups: Sham, Blank gel, DOX bolus (2.5 mg/kg), DOX@gel (2.5 mg/kg), DOX bolus (0.25 mg/kg), DOX@gel (0.25 mg/kg), RAcNPs@gel (1 mg/kg), GM-CSF gel (20 μg/kg), DOX (0.25 mg/kg)/RAcNPs (1 mg/kg)/GM-CSF gel (20 μg/kg), three mice in each group. During the trial, deaths were recorded. After the experiment, the brains were dissected and HE-stained sections were prepared for histopathological analysis. To confirm that intracranial chemotherapy reduces systemic toxicity compared with intravenous administration, healthy mice were divided into three groups of 3 mice each. One group of mice was intracranially administered DOX&RAcNPs@GM gel at a dose of 0.25 mg/kg DOX. Another group of mice received intravenous-free DOX on days 4, 8, and 12 at a dose of 10 mg/kg. Mice intravenously injected with PBS were set as a control group. Two weeks after the treatment period, blood samples were collected for hematology analysis and HE-stained sections of major organs (heart, lung, spleen, liver, and kidney) were prepared for histopathological examination.

### 2.17. Statistical analysis

All data are expressed as the mean ± standard deviation (SD). Two-tailed Student's *t*-tests were used for statistical analysis. Statistical differences were defined as $^*P < 0.05$, $^{**}P < 0.01$, and $^{***}P < 0.001$. The abbreviation "ns" represented no significant difference between groups.

## 3. Results

### 3.1. Inevitable recurrence of GBM

We reviewed the brain MRI images of GBM patients with surgeons and found that most GBM is highly infiltrative and invasive, with indistinct and irregular borders to normal brain tissue (Fig. 1D). This phenomenon greatly complicates clinical surgical resection. Infiltrating tumor cells inside the brain parenchyma cannot be completely excised because of the damage to a healthy brain. To study tumour recurrence after surgery, an orthotopic GBM C6 model was established. Several small islands of tumor cells remained around the cavity after excision (Supporting Information Fig. S1A) and an apparent recurrence was observed 14 days post-surgery (Fig. S1B). Therefore, postoperative intervention is critical to inhibit glioma recurrence.

### 3.2. Characterization of DOX/RAcNPs@GM gel

Clinical studies have confirmed that R837, as a toll-like receptor 7 agonists, can promote the maturation and antigen presentation of DCs in glioma patients[30,31]. Given the poor solubility of R837, the encapsulation of nanoparticles has been shown to help improve the distribution and effectiveness of the drug[28,32]. RAcNPs and PEGylated nanoparticles (PEG-NPs) were prepared by emulsification-diffusion method[27,28], with an average particle size of 120 nm (Supporting Information Fig. S2A) and negative surface charges (Fig. S2B). Transmission electron microscope (TEM) images showed a spherical appearance and narrow size range of various NPs (Fig. 2A and Fig. S2C). Long-term stability

experiments confirmed that RAcNPs were stable in PBS for more than 3 weeks, despite the absence of a PEG hydration layer (Supporting Information Fig. S3).

The rapid clearance at the administration site hinders the sustained activation of immune signaling. Therefore, DOX, RAcNPs, and GM-CSF were further encapsulated in biodegradable alginate (ALN) hydrogel to obtain an injectable immune activation system (Fig. 2B). We first examined the *in vitro* safety of three components. The hemolysis experiment confirmed the biosafety of DOX, RAcNPs, and GM-CSF (Supporting Information Fig. S4). Fluidic ALN can match irregular brain wounds and gelatinize spontaneously and rapidly in the presence of physiological calcium ions (Fig. 2C). Based on the hydrodynamic properties and the gelatinization conditions of ALN, we envision developing a handheld spray containing both $CaCl_2$ and ALN that quickly gelatinizes through simultaneous spraying and mixing to match a variety of irregular wounds (Fig. 2E). Scanning electron microscope (SEM) images substantiated the formation of ALN hydrogel with a porous network structure (Fig. 2D) and confocal laser scanning microscopy (CLSM) images indicated the homogeneous distribution of RAcNPs in ALN hydrogel (Fig. 2F).

DOX is beneficial for killing residual tumour cells in a timely manner while GM-CSF and RAcNPs are conducive to eliciting durable immune responses. Next, we investigated the release profiles of DOX, GM-CSF, and RAcNPs from the hydrogels with different ALN concentrations (Fig. 2G). As expected, the three substances were released from hydrogel in an ALN concentration-dependent manner. The degradation and release rate of hydrogel slowed down with the increase of ALN concentration (Supporting Information Fig. S5), indicating that ALN hydrogel is a good drug delivery carrier with an extended-release period.

### 3.3. DOX/RAcNPs enhance GBM immunogenicity

Anthracycline-treated tumour cells are generally resultful at improving anti-tumour immune responses by facilitating TAAs exposure and damaging associated molecular molecule pattern (DAMP) release (Fig. 3A)[33]. To verify the feasibility of this dogma on GBM, a cytotoxicity analysis of DOX was first performed. Shown in Fig. 3B and Supporting Information Fig. S6, DOX displayed potent broad-spectrum cytotoxicity against various GBM cells, including human and mouse cell lines, in a dose- and time-dependent manner. CLSM images revealed rapid proapoptotic translocation of calreticulin (CRT) to the cell surface after a brief incubation with DOX (Fig. 3C), an "eat me" signal that triggers the recognition and clearance by APCs[34,35]. Meanwhile, DOX treatment induced a significant extracellular release of high-mobility group box 1 (HMGB1, Fig. 3D), a DAMP that plays a key role in mediating inflammatory reaction and DCs maturation[36]. Also, immunofluorescence analysis confirmed that intracranial administration of DOX could induce GBM apoptosis and CRT exposure *in vivo* (Supporting Information Fig. S7), consistent with the results of *ex vitro* tests.

Next, we sought to verify our initial hypothesis that RAcNPs could affect the recognition and cytoplasmic delivery of antigens released after DOX treatment to maximize amplify immunogenic signals (Fig. 3A). Green fluorescent protein (GFP) was used as a detectable intracellular antigen and RAcNPs were labeled with DID, a dye that emits red fluorescence. After incubation with tumour antigens for 2 h, the total amount of protein bound by each nanoformulation was first quantified. As displayed in Fig. 3E, RAcNPs, and AcNPs successfully captured a larger number of antigen proteins. Qualified and quantitative analysis obtained by CLSM images and flow cytometry further demonstrated the improved cytoplasmic delivery of antigen upon capture by AcNPs compared with free antigens, regardless of R837 loading (Fig. 3F and G). However, the PEG layer interfered with the adsorption and subsequent intracellular delivery of antigens. Taking into account the physicochemical characteristics and the results of *ex vitro* cell experiments, RAcNPs, instead of PEG-NPs, should be used in subsequent tests. A large number of DCs emitting both red and green fluorescence were detected by flow cytometry (Supporting Information Fig. S8), indicating the successful co-delivery of antigens and NPs by RAcNPs. More importantly, DOX combined with RAcNPs significantly upregulated the expression of CD80/86 on the surface of bone marrow DCs (BMDCs, Fig. 3H and I and Supporting Information Fig. S9), compared with DOX or RAcNPs alone, demonstrating the complete mature and activation of DCs. These results confirm that DOX in collaboration with RAcNPs effectively promotes tumor antigen exposure and subsequent delivery of this dangerous antigen signal to DCs.

### 3.4. GM-CSF hydrogel prolongs drug retention and increases the immune infiltrates

The rapid clearance at the administration site hinders the sustained activation of immune signaling, hence we investigated the intracranial retention behavior of DOX, RAcNPs, and GM-CSF. DOX, DiD-labelled RAcNPs, and GM-CSF were either dispersed in PBS (bolus) or encapsulated in ALN hydrogel which was subsequently injected into the brain. The residual DOX and RAcNPs were monitored by an *in vivo* imaging spectrum system (IVIS) and GM-CSF was determined by an ELISA kit. The encapsulation by ALN hydrogel, as shown, greatly prolonged the intracranial residence of three drugs. While 97.6% of the signal from the RAcNPs bolus was undetectable at the injection site on Day 8, 70.5% of that from RAcNPs@gel remained detectable (Fig. 4A, C and Supporting Information Fig. S10). DOX@gel exhibited analogous prolonged retention at the injection site on Day 12, though the signals from DOX bolus almost disappeared (Fig. 4B). Similarly, the concentration of GM-CSF was 38.7-fold higher in the GM-CSF gel group than that in the GM-CSF bolus group 72 h after injection (Fig. 4E and F). Collectively, ALN hydrogel is a good candidate for the sustained release of multiple drugs.

The priming of anti-tumour immune response is a sophisticated process that requires multiple stimulatory signals originating from DCs[37,38]. Next, we sought to verify the other initial hypothesis that GM−CSF−loaded hydrogel can amplify the chemotactic signal, and attract and increase the intracranial DCs infiltration (Fig. 4D). As key initiators of anti-tumour immune responses, an increase in the number of DCs in the brain was determined by immunohistochemical analysis on Day 6 post-injected with GM-CSF gel (Fig. 4E). The number of DCs in the brains of mice treated with GM−CSF-loaded hydrogel was 2.9 times that of mice treated with blank hydrogel (Fig. 4G), demonstrating the feasibility of intracranial cytokine administration strategy.

### 3.5. DOX/RAcNPs synergistic with GM-CSF to enhance immune responses

Adequate intracranial DCs infiltration and enhanced antigen presentation are both critical for triggering maximum anti-GBM immunity. Therefore, we next investigated whether DOX/RAcNPs combined with GM-CSF can improve adaptive immunity

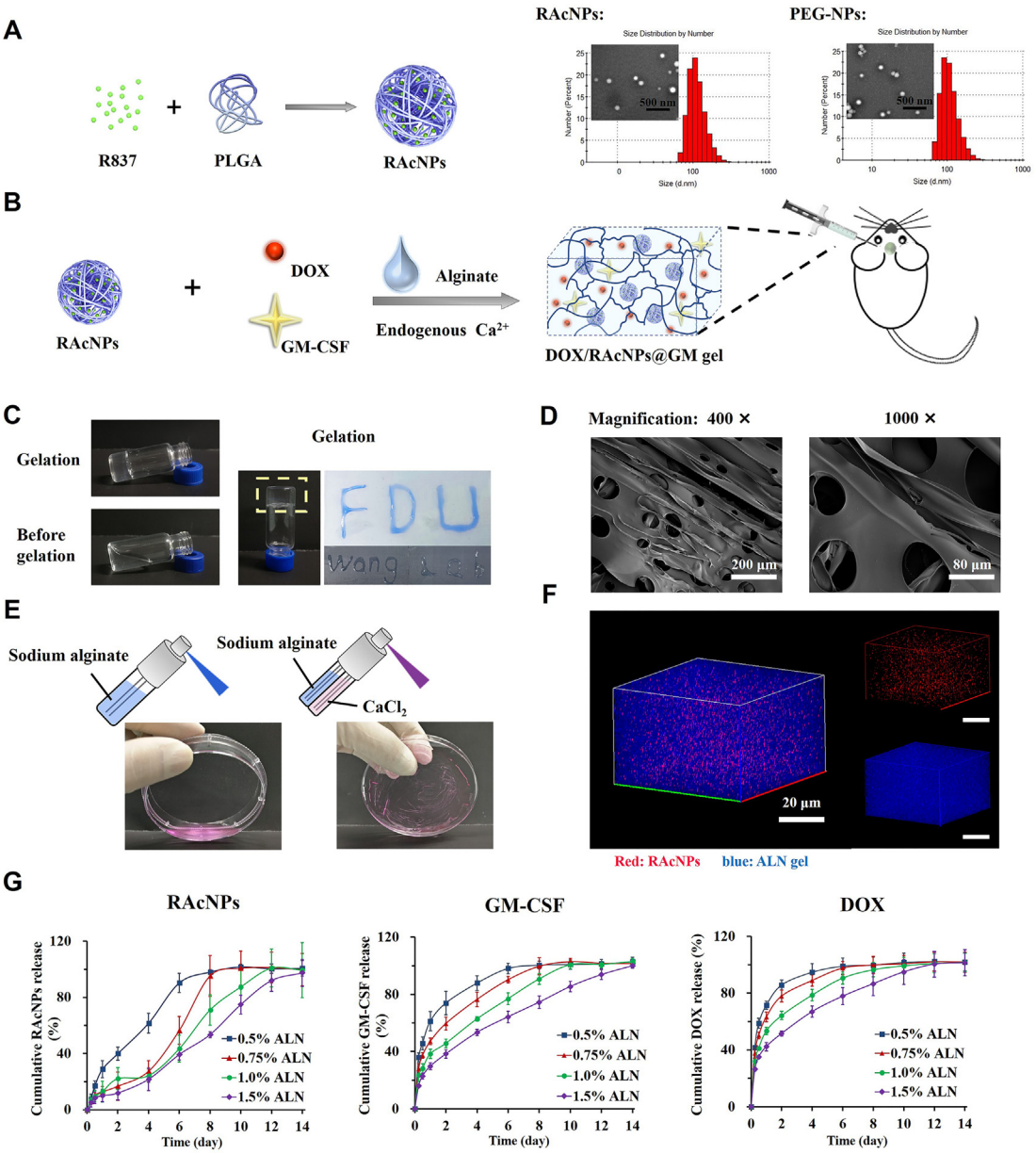


**Figure 2** Design and characterization of DOX/RAcNPs@GM gel as a drug-delivery depot. (A) Preparation and particle size of RAcNPs and PEG-NPs. (B) Schematic illustration of ALN hydrogel for the encapsulation of DOX, RAcNPs, and GM-CSF. (C) Representative photographs of ALN hydrogel and the formation of diverse geometric shapes after syringe injection. ALN gelatinizes rapidly after cross-linking with calcium ions. (D) Representative scanning electron microscope images of ALN hydrogel. Scale bar, 200 μm (left) and 80 μm (right). (E) Representative images of thin films formed by simultaneous spraying of ALN and calcium chloride solutions. (F) Confocal microscopy images of the uniform distribution of RAcNPs in ALN hydrogels. Scale bar, 20 μm. (G) Release profiles of each agent from DOX/RAcNPs@GM gel. Data are presented as mean ± SD ($n = 3$). Two-tailed Student's *t*-test were used for statistical analysis.

(Fig. 5A). Inflammatory cytokines and the expansion of immune responders—T lymphocytes were analyzed on Day 11 after various treatments. Shown in Fig. 5B, more helper T cells ($CD3^+CD4^+$) and cytotoxic T cells ($CD3^+CD8^+$) were detected in the mice treated with DOX/RAcNPs loaded GM-CSF hydrogel (DOX/RAcNPs@GM gel) than those with PBS or DOX/RAcNPs without GM-CSF. Meanwhile, the intracerebral interferon-γ (IFN-γ) concentration in DOX/RAcNPs@GM gel group was much higher than other groups without GM-CSF (Fig. 5C and D), indicating a compensatory improvement in immune infiltration mediated by DOX/RAcNPs and GM-CSF.

### *3.6. Therapeutic efficacy of DOX/RAcNPs@GM gel on recurrent GBM*

The above results have confirmed that DOX/RAcNPs can enhance GBM immunogenicity, while GM-CSF can increase intracranial immune infiltrates. In the next step, we investigated the synergistic effect of both of them on GBM recurrence. A safe dose of the drug is the key to its therapeutic effect. We first carried out an acute toxicity analysis to opt for a safe dose. Following intracranial administration of 2.5 mg/kg DOX, several mice died during the experiment, but deaths were averted and no cerebral hemorrhage

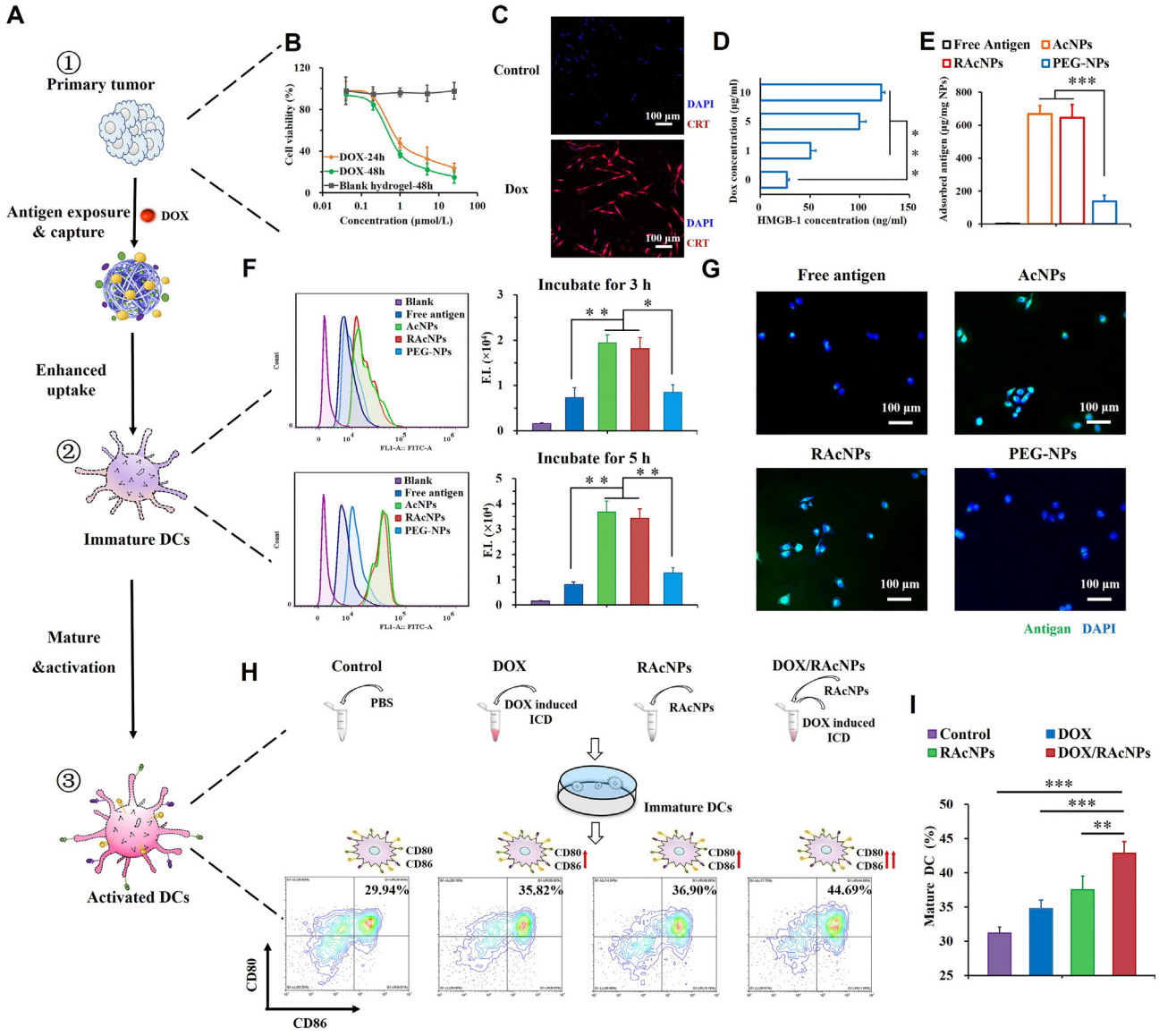


**Figure 3** DOX/RAcNPs enhance GBM immunogenicity. (A) Schematic illustration of antigens exposure and DCs activation triggered by DOX/RAcNPs. (B) Cytotoxicity analysis of DOX on C6 GBM cells ($n = 4$). (C) Fluorescent images of CRT exposure on the surface of C6 cells after DOX treatment. Scale bar, 100 μm. (D) HMGB-1 release from GBM cells treated with various concentrations of DOX ($n = 4$). (E) The amount of antigen adsorbed by various NPs ($n = 6$). (F) Flow cytometry analysis and (G) confocal microscopy images of DC cells after incubation of various preparations. Blue, cell nuclei; green, GBM antigens. Scale bar, 50 μm. (H) Flow cytometry and (I) quantitative analysis of matured DCs after various stimuli. Mice bone marrow DCs expressing both CD80 and CD86 were selected and defined as mature DCs ($n = 4$). (B, C, D, E, I) Data are presented as mean ± SD. Two-tailed Student's *t*-test were used for statistical analysis. $^{**}P < 0.01$, $^{***}P < 0.001$.

or injury was observed when the DOX dose was reduced to 0.25 mg/kg (Supporting Information Figs. S11A and B). Acute toxicity of intracranial injections of RAcNPs and GM-CSF was also investigated. As expected, the two components were safe and did not negatively affect the mice's health or behavior. Therefore, the doses of DOX, R837, and GM-CSF for intracranial administration were 0.25 mg/kg, 1 mg/kg, and 20 μg/kg, respectively.

To evaluate the suppressed effect of DOX/RAcNPs@GM gel on GBM regrowth, an orthotopic C6 tumour model was established. On Day 14 after tumour engraftment, the gross tumour mass was surgically resected and hydrogel was injected into the cavity (Fig. 6A and C). IVIS imaging notarized the successful excision (Fig. 6B). The bioluminescence of glioma cells after surgical resection is almost impossible to detect. MRI is the gold standard for clinical GBM diagnosis and postoperative recurrence monitoring. Using MRI procedures, we visualized the morphology of intracranial tumors in rats (Fig. 6D). Also, we periodically monitored the development of recurrent GBM by a 3T nuclear MRI system. As shown in Fig. 6E, aggressive growth of the tumour was observed in the rats without any treatment (Control group). In addition, tumours in rats treated with TMZ also grew barbarically, with a negligible remission of GBM progression compared with the control group. The rats treated with DOX/RAcNPs@gel displayed reduced tumour volume on Day 8 post-surgery (Fig. 6F; $P = 0.0480$ compared with the control group). Nevertheless, tumours continued to grow and all

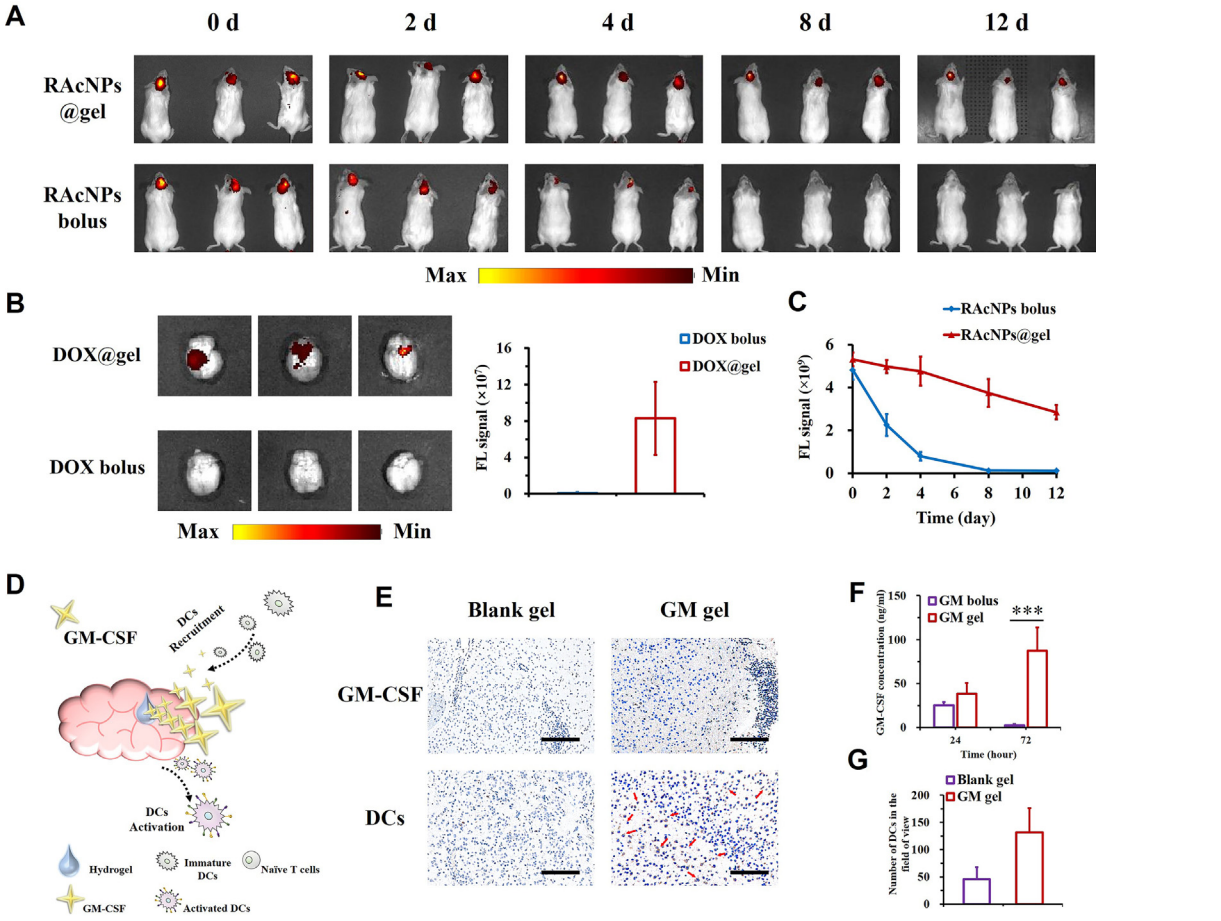


**Figure 4** GM-CSF hydrogel prolongs drug retention and increases the immune infiltrates. (A) Real-time *in vivo* fluorescence imaging of mice injected with RAcNPs@gel or RAcNPs bolus. (B) *Ex vivo* fluorescence imaging of mice 12 days after injection of DOX@gel or DOX bolus. (C) Quantitative analysis of residual fluorescence intensity of RAcNPs. (D) Interpretation of GM−CSF−loaded hydrogel increasing intracranial DCs infiltrates. (E) Immunochemical analysis of mouse brain after injection of blank gel or GM-CSF gel. Scale bar, 200 μm. (F) Brain GM-CSF concentration in mice treated with GM-CSF bolus or GM-CSF gel. (G) The number of DCs in brain slices. (B, C, F, G) Data are presented as mean ± SD ($n = 3$). Two-tailed Student's *t*-test were used for statistical analysis. ***$P < 0.001$.

rats died within 32 days after surgery, presumably attributed to the insufficient immune infiltrates in the tumor site. In contrast, the rats receiving DOX/RAcNPs@GM gel provided durable tumour suppression, covering both early and late stages of GBM recurrence (Fig. 6F). Tumour volumes throughout the experimental period were much smaller than those in control ($P = 0.0149$ on Day 20 post-surgery) or TMZ group ($P = 0.0247$ on Day 20 post-surgery).

Inspired by the successful anticancer effect against the GBM model, we further investigated the immune response underlying the observed therapeutic efficacy of DOX/RAcNPs@GM gel. The concentrations of IFN-γ, interleukin-2 (IL-2), IL-10, and transforming growth factor-β (TGF-β) in the tumour site were determined to investigate the enhanced anti-tumour immune responses and attenuated immunosuppressive signaling (Fig. 7A and B). The levels of IFN-γ, which promote T-cell responses by stimulating the antigen processing and presentation machinery, were found to be about 2.1−3.2-fold higher in rats receiving DOX/RAcNPs@GM gel than those in the control groups (Fig. 7A). DOX/RAcNPs@GM gel also elevated the concentration of IL-2, but an opposite trend was found for IL-10 and TGF-β. A slight decrease for intracranial TGF-β and an obvious shrinkage for IL-10 were detected in the rats in DOX/RAcNPs@GM gel group (Fig. 7A). Meanwhile, tumors were further collected and the immune infiltration was analyzed by immunofluorescence (Fig. 7C). An enhanced $CD11c^+$ DCs infiltration in GBM microenvironment of DOX/RAcNPs@GM gel group was first observed. The number of $CD8^+$ cytotoxic T cells in the GBM microenvironment was greatly increased after intracranial administration of DOX/RAcNPs@GM gel, which was much higher than that in other groups. DOX/RAcNPs@GM gel could also increase the frequency of $CD4^+$ helper T cells.

All the above results demonstrated that an intracavity injection of immune-amplified hydrogel in a postoperative model could not only enhance the GBM immunogenicity but also increase intracranial immune infiltrates, ultimately resulting in a durable and potent immune response for the suppression of full-stage GBM regrowth.

### 3.7. *Biosafety evaluation*

Systemic injection of DOX is known to cause severe myelosuppression and heart, liver, kidney, and testicular damage. We hope to investigate whether systemic toxicity and myelosuppression could

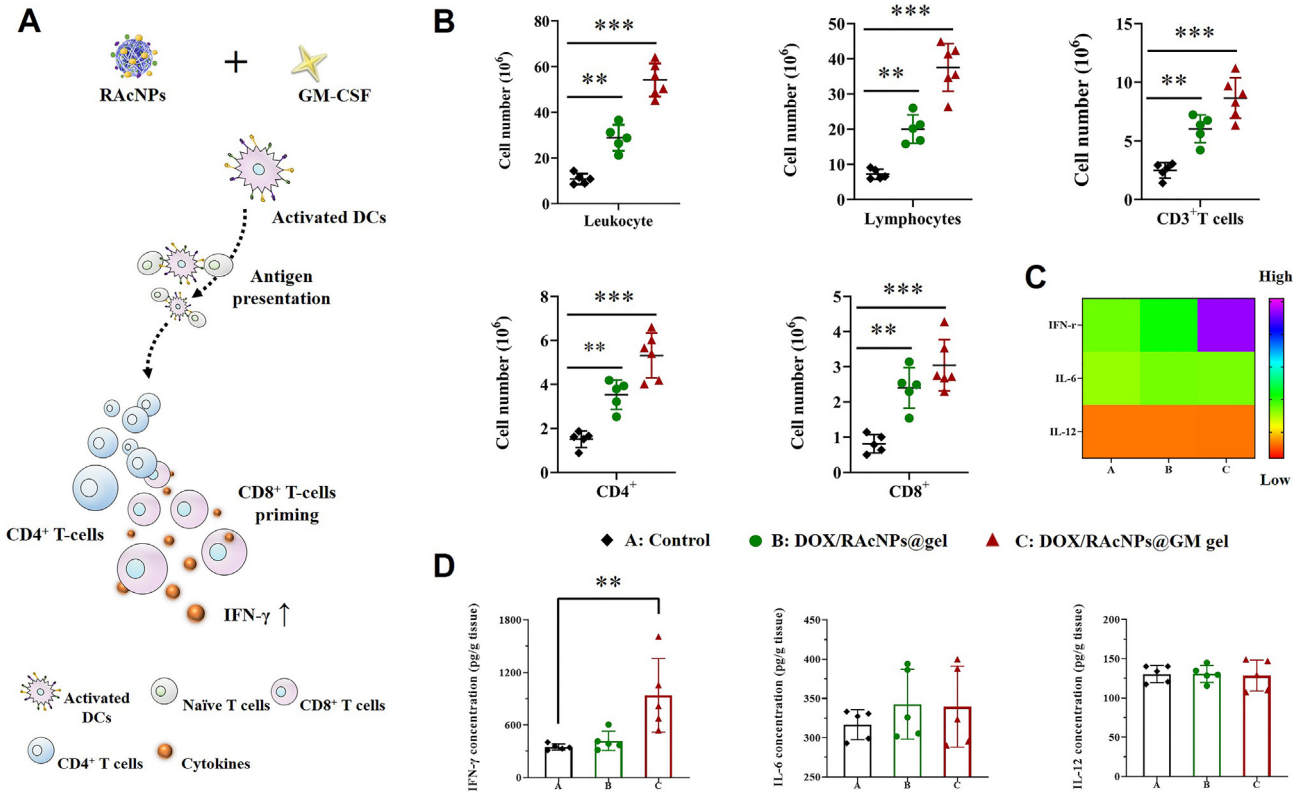


**Figure 5** DOX/RAcNPs synergistic with GM-CSF to enhance immune responses. (A) Interpretation of improved immune response. (B) The number of lymphocytes in mice intracranially injected with PBS, DOX/RAcNPs@gel, or DOX/RAcNPs@GM gel. (C, D) The concentration of brain inflammatory cytokines in mice intracranially injected with PBS, DOX/RAcNPs@gel, or DOX/RAcNPs@GM gel. Data are presented as mean ± SD ($n = 5$). Two-tailed Student's $t$-test were used for statistical analysis. $^{**}P < 0.01$, $^{***}P < 0.001$.

be avoided by topical administration of hydrogel encapsulated chemotherapeutic drugs DOX and other immune promoters (RAcNPs and GM-CSF). After different treatments, blood samples were collected for hematology analysis, and HE-stained sections were prepared for histopathological analysis. Compared with the drastic decrease in blood leukocytes and severe splenic and renal toxicity in mice after intravenous administration of DOX, mice were in good condition after intracranial injection of DOX/RAcNPs@GM gel at the doses of 0.25 mg/kg DOX, 1 mg/kg RAcNPs and 20 μg/kg GM-CSF. After DOX/RAcNPs@GM gel treatment, no injuries were observed in the brain, heart, lung, spleen, liver, kidney, and other major organs, and no significant changes in the number of white blood cells were detected (Fig. S11C, D and E). The results were confirmed by hematology analysis and histopathological examination (Supporting Information Table S1).

### *3.8. Development of an extracranially administered immune-amplifying vaccine for non-invasive treatment of unresectable multiple GBM*

Intracranially administrated chemo-immune hydrogels confer great benefits in postoperative GBM therapy, however, the topical regimen is feeble towards unresectable systemic metastases or multiple lesions. Therefore, we utilized the antigen capture property of RAcNPs and the DCs recruitment ability of GM-CSF to construct an immuno-amplifying vaccine that triggers potent humoral and T-cell responses to treat unresectable multiple GBM by extracranially enriching, reprogramming, activating, and releasing DCs (Fig. 8A). GBM-lysed antigens were first captured by RAcNPs to fabricate nanovaccines (NanoVac) and further encapsulated into a GM−CSF-loaded hydrogel (NanoVac@GM gel).

We first evaluated the therapeutic efficacy of NanoVac@GM gel on a multiple diffuse GBM model (Fig. 8B). Mice were in poor condition after successful model establishment. Mice given NanoVac@GM gel exhibited significantly longer median survival than other groups (Fig. 8C). Tumor volume quantified by MRI further identified that the prolonged survival could be attributed to the suppression of intracranial tumor growth (Fig. 8D). Furthermore, we evaluated the systemic immune activation mediated by NanoVac@GM gel. The frequency of spleen lymphocytes and the serum cytokines level was measured to determine the strength of the systemic anti-GBM response. Seven days after different treatments, serum IFN-γ and TNF-α concentration and spleen T lymphocytes were determined by ELISA kits or flow cytometry, respectively. A higher number of spleen matured DCs, $CD4^+$ and $CD8^+$ T cells (Fig. 8F), and an elevated IFN-γ and TNF-α level (Fig. 8E) were found in NanoVac@GM gel-vaccinated mice compared with those in the mice treated with GM@gel or NanoVac@gel.

## 4. Discussion

GBM is the most aggressive and malignant brain tumour. The standard therapy for GBM clinically is surgical resection followed

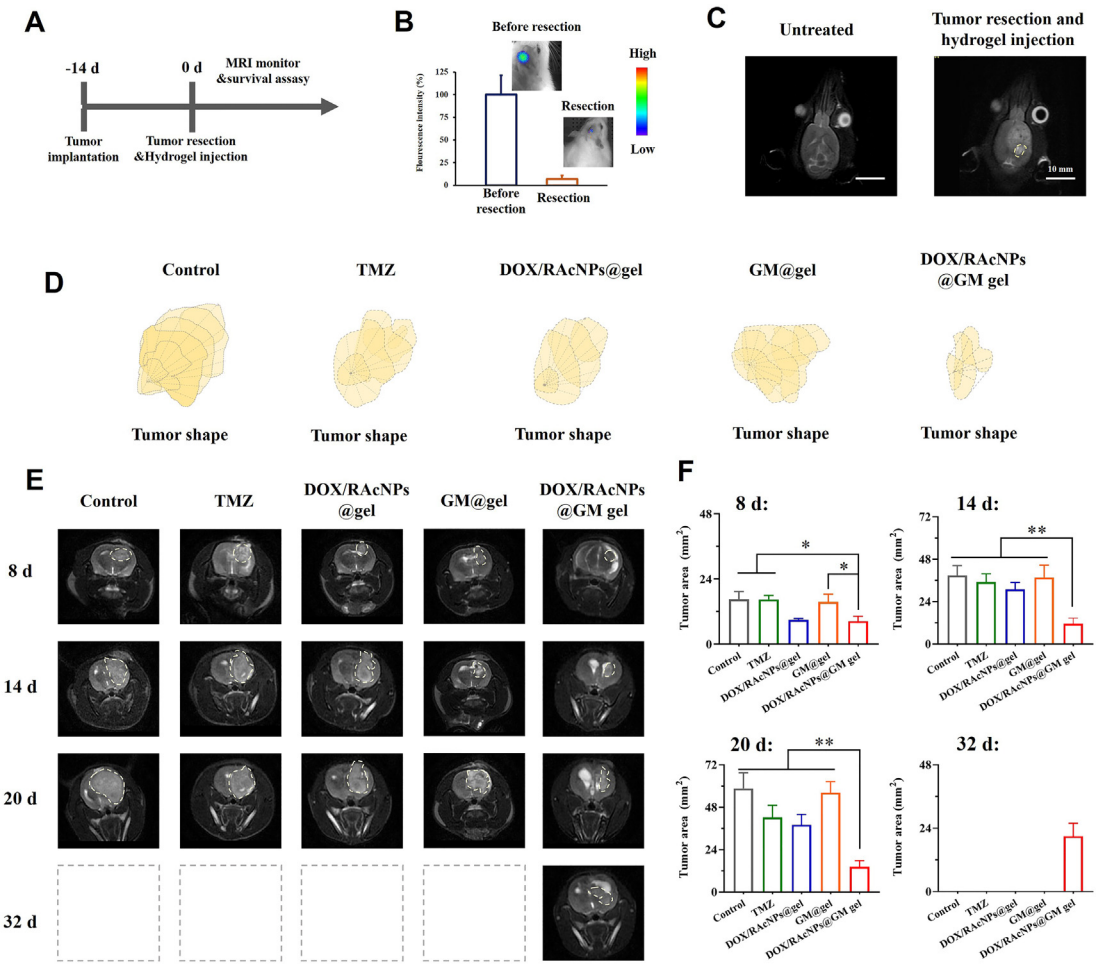


**Figure 6** Therapeutic efficacy of DOX/RAcNPs@GM gel on recurrent GBM. (A) The therapeutic schedule for recurrent GBM. Mice were surgically resected with tumour mass on Day 14 after engraftment and received various treatments. (B) *In vivo* fluorescence of mice underwent surgical excision. (C) Image of mice with or without *in situ* hydrogel injection. (D) The shape of intracranial tumors reconstructed by MRI images. (E) MRI images (F) and quantitative analysis of tumour area in GBM-bearing mice after different treatments. Data are presented as mean ± SD ($n = 3$). Two-tailed Student's *t*-test were used for statistical analysis. $^{*}P < 0.05$, $^{**}P < 0.01$.

by radiotherapy and adjuvant chemotherapy, such as oral TMZ. Nevertheless, the median survival remains 15 months[39]. Relative to other tumour types, GBM shows scarce tumour-infiltrating APCs and other immune effector cells[40]. A large number of failed cases of GBM immunotherapy support this verdict. A phase III trial (CheckMate-143) comparing the immune checkpoint inhibitor nivolumab with angiogenesis inhibitor bevacizumab in the treatment of recurrent GBM show no overall survival (OS) benefit[41]. Another phase III trial announced in 2019 (CheckMate-498, NCT02617589) also failed to obtain OS advantage in newly diagnosed O6-methylguanine-DNAmethytransferase promoter-unmethylated GBM patients[42]. In that trial, nivolumab combined with radiation was compared with TMZ plus radiation.

Incentivized by promising initial results, DCs-base vaccines have been explored in pediatric and adult patients with GBM for decades. These DCs-based vaccination approaches, ordinarily, require *ex vivo* cell isolation and activation, followed by the introduction of these programmed cells into GBM patients to enhance responses[43,44]. Aside from the high cost, numerous open questions remain to be addressed to guarantee the therapeutic efficacy of this sophisticated process[45,46]. For one, more than 90% of cells die during transplantation and few succeed in homing to the LNs[47,48]. In contrast to vaccines that rely on such a tedious *ex vivo* procedure to modulate DCs, GM−CSF-loaded biomaterial scaffold imitates an infection environment to enrich a large number of immature DCs *in situ* for antigen recognition and loading[49]. DCs, the most potent APCs in our body, has been identified as recruited and proliferated by GM-CSF. Such biological scaffolds provide a suitable platform to manipulate, directly in the body, DCs recruitment, maturity, and finally emigration to LNs[16,50] and a promising strategy for the treatment of various malignancies[51−54]. In this investigation, a porous ALN hydrogel was developed as a drug reservoir and residence for DCs mature. Crosslinked with calcium ions and gelatinized quickly *via* local administration, ALN is a kind of natural polysaccharide widely used in tissue engineering and drug-controlled release[55,56]. This injectable pore-forming hydrogel, composed of a bulk and porous network, involves simple preparation, minimally invasive delivery, biodegradable properties, tunable release kinetics through modulation of molecular weight and concentration, as well as ready incorporation of a wide array of therapeutics[57].

In this study, we attempted to fabricate a chemoimmunotherapy-based ALN hydrogel releasing DOX, RAcNPs, and GM-CSF to actively recruit DCs and subsequently

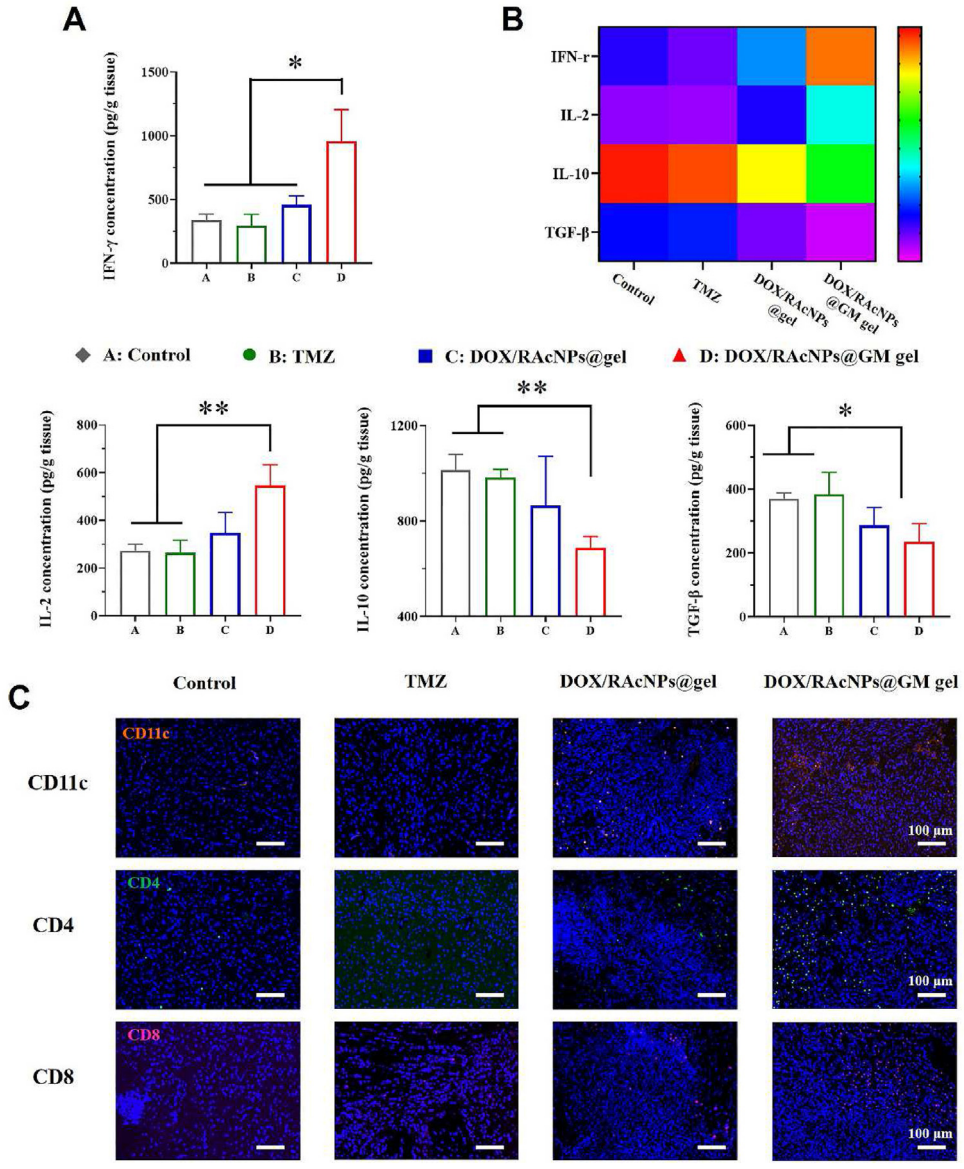


**Figure 7** DOX/RAcNPs@GM gel mediates antitumor immune recovery on relapsed GBM. (A) quantitative analysis and (B) heatmap of cytokine levels in brain tumours. Data are presented as mean ± SD ($n = 4$). Two-tailed Student's $t$-test were used for statistical analysis. $^{*}P < 0.05$, $^{**}P < 0.01$, $^{***}P < 0.001$. (C) Immunofluorescence analysis of brain tumours after various treatments. Blue, cell nuclei; orange, $CD11c^{+}$ DCs; green, $CD4^{+}$ T cells; pink, $CD8^{+}$ T cells, scale bar = 200 μm.

elicit a durable anti-tumour response, and confirmed its therapeutic effect on a recurrent GBM model. A variety of approaches, including photothermal therapy[58,59], radiation therapy[32], ultrasound therapy[60], and chemotherapy[61] have been explored as means to boost the response rate of many "cold" tumour. However, myelosuppression, one of the serious complications of current systemic chemotherapy and radiotherapy regimens, causes life-threatening neutropenia and thrombocytopenia and hinders the deployment of oncology treatments[62]. The same rule applies to oral TMZ. Patients receiving TMZ, especially in intensified dose regimens, are immunosuppressed and have an increased incidence of opportunistic infections[22,23]. In our work, the locally administered chemoimmunotherapy regimen circumvents this problem. No decrease in blood leukocytes or damage to major organs, but a promoted anti-tumour response was observed in mice receiving an intracranial injection of DOX/RAcNPs@GM gel. Histopathological examination and hematology assays confirmed the biosafety and immunochemical analysis determined the enhanced intracranial immune response of DOX/RAcNPs@GM gel.

Enlightened by nanomaterial-based tumour vaccines, we developed an antigen-captured nanovaccine to further improve the immunogenicity of GBM. Nanomaterials have been extensively validated to enhance intracellular delivery of therapeutics[63–67], especially biological macromolecules[68], and immune signaling[69–71]. R837 is a TLR-7 ligand, which could remarkably upregulate the expression of intercellular adhesion molecule-1 and induce the secretion of a variety of inflammation cytokines[72]. The co-delivery of TAAs and TLR agonists by the same NPs promotes antigen internalization, process, and presentation, which is crucial to induce tumour-specific T-cell responses[73]. Moreover, further

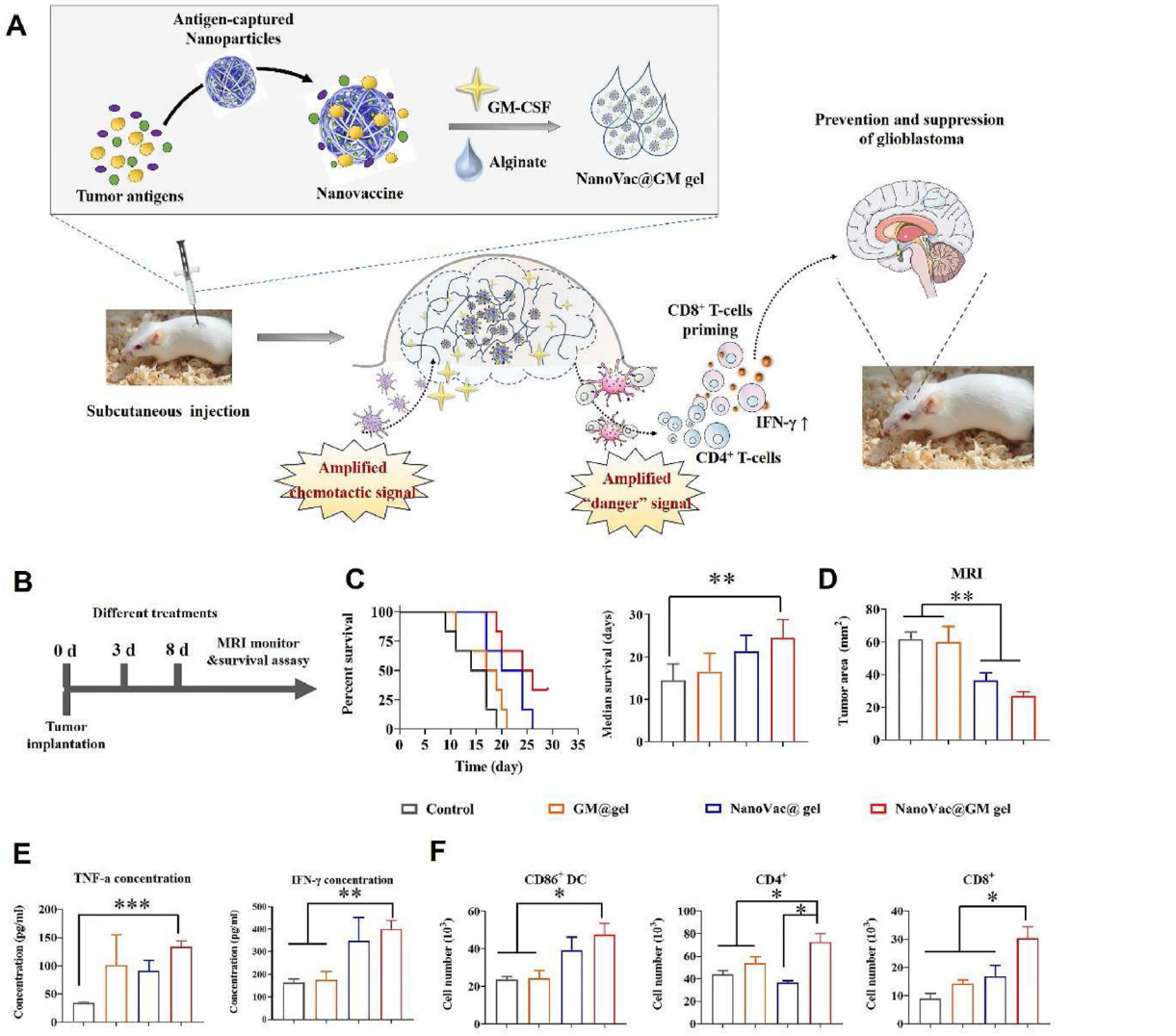


**Figure 8** Non-invasive treatment of NanoVac@GM gel against orthotopic multiple GBM. (A) Schematic illustration of NanoVac@GM gel that triggers potent humoral and T-cell responses by extracranially enriching, reprogramming, and releasing DCs. (B) The therapeutic schedule for unresectable multiple GBM. (C) Survival of mice with multiple GBM. (D) Quantitative analysis of tumour area based on MRI imaging. (E) Serum cytokines level in mice after immunization ($n = 4$). (F) The number of DCs and T lymphocytes in mice spleen after immunization ($n = 3$). Data are presented as mean ± SD. Two-tailed Student's *t*-test were used for statistical analysis. $^{*}P < 0.05$, $^{**}P < 0.01$, $^{***}P < 0.001$.

loaded into the three-dimensional and porous ALN hydrogel, NanoVac@GM gel provided a sustained release of GM-CSF to concentrate a good deal of DCs with distinct subsets, and the co-delivery antigens and TLR agonists to program DCs to elicit anti-GBM responses.

## 5. Conclusions

Immunotherapy for GBM remains a formidable challenge in the clinic. Relative to other tumour types, GBM shows scarce tumour-infiltrating DCs and other immune effector cells[40]. A large number of failed cases of GBM immunotherapy support this verdict. In this work, we attempted to fabricate a chemoimmunotherapy-based ALN hydrogel slowly releasing DOX, RAcNPs, and GM-CSF to actively recruit DCs and subsequently elicit a durable anti-tumour response. We confirmed the excellent therapeutic effect of this immune-amplifying hydrogel on a recurrent GBM model. Additionally. the locally administered chemoimmunotherapy regimen circumvents the myelosuppression and other side-effect caused by current systemic chemotherapy effectively. To conclude, this study describes a biomaterial-based immune-amplification device loaded with RAcNPs and GM-CSF, which has achieved good results in both postoperative recurrent and multiple GBM models.

## Acknowledgments

This work was supported by the National Natural Science Foundation of China (No.81773911, 81690263, and 81573616), and the Development Project of Shanghai Peak Disciplines-Integrated Medicine (No.20180101). We thank Shengsheng Xie and the staff of the National Facility for Protein Science in Shanghai (NFPS) for valuable technical support. We sincerely thank Qiuyue Han and Yuqi Zhu for their great help with MRI imaging, Songlei Zhou and Yiwen Zhang for their guidance on the establishment of the recurrent GBM model, Yihui Deng and Huining He for their

experience in immunotherapy, and Mengting Yang for the guidance on GBM cell culture.

## Author contributions

Qiujun QIU contributed to the study design, data acquisition, and manuscript writing. Sunhui Chen contributed to the establishment of GBM model. Dongdong Wang and Bo Yin were in charge of MRI imaging and image analysis. Jixiang Chen, Xinyi Ding, Jiangang Yang, Pengcheng Guo, Chao Gao and Jixiang Chen assisted in the performance of animal experiments. Yang Li and Jisu Kim contributed to data analysis and interpretation. Shihao Zheng guided the method of GBM resection. Huining He, Jianyong Sheng and Jianxin Wang developed the concept and supervised experiments.

## Conflict of interest

The authors have no conflicts of interest to declare.

## Appendix A. Supporting information

Supporting data to this article can be found online at https://doi.org/10.1016/j.apsb.2023.06.010.

## References


1. de Robles P, Fiest KM, Frolkis AD, Pringsheim T, Atta C, St Germaine-Smith C, et al. The worldwide incidence and prevalence of primary brain tumors: a systematic review and meta-analysis. *Neuro Oncol* 2015;**17**:776−83.
2. Park JK, Hodges T, Arko L, Shen M, Iacono DD, McNabb A, et al. Scale to predict survival after surgery for recurrent glioblastoma multiforme. *J Clin Oncol* 2010;**28**:3838.
3. Hamard L, Ratel D, Selek L, Berger F, van Der Sanden B, Wion D. The brain tissue response to surgical injury and its possible contribution to glioma recurrence. *J Neuro Oncol* 2016;**128**:1−8.
4. Xue J, Zhao Z, Zhang L, Xue L, Shen S, Wen Y, et al. Neutrophil-mediated anticancer drug delivery for suppression of postoperative malignant glioma recurrence. *Nat Nanotechnol* 2017;**12**:692.
5. Garon EB, Rizvi NA, Hui R, Leighl N, Balmanoukian AS, Eder JP, et al. Pembrolizumab for the treatment of non-small-cell lung cancer. *N Engl J Med* 2015;**372**:2018−28.
6. Robert C, Thomas L, Bondarenko I, O'Day S, Weber J, Garbe C, et al. Ipilimumab plus dacarbazine for previously untreated metastatic melanoma. *N Engl J Med* 2011;**364**:2517−26.
7. Sampson JH, Gunn MD, Fecci PE, Ashley DM. Brain immunology and immunotherapy in brain tumours. *Nat Rev Cancer* 2020;**20**:12−25.
8. Lim M, Xia Y, Bettegowda C, Weller M. Current state of immunotherapy for glioblastoma. *Nat Rev Clin Oncol* 2018;**15**:422−42.
9. Friedrich M, Sankowski R, Bunse L, Kilian M, Green E, Ramallo Guevara C, et al. Tryptophan metabolism drives dynamic immunosuppressive myeloid states in IDH-mutant gliomas. *Nat Can (Que)* 2021;**2**:723−40.
10. Weller M, Roth P, Preusser M, Wick W, Reardon DA, Platten M, et al. Vaccine-based immunotherapeutic approaches to gliomas and beyond. *Nat Rev Neurol* 2017;**13**:363−74.
11. Goldmann J, Kwidzinski E, Brandt C, Mahlo J, Richter D, Bechmann I. T cells traffic from brain to cervical lymph nodes *via* the cribroid plate and the nasal mucosa. *J Leukoc Biol* 2006;**80**:797−801.
12. Aspelund A, Antila S, Proulx ST, Karlsen TV, Karaman S, Detmar M, et al. A dural lymphatic vascular system that drains brain interstitial fluid and macromolecules. *J Exp Med* 2015;**212**:991−9.
13. Barry KC, Hsu J, Broz ML, Cueto FJ, Binnewies M, Combes AJ, et al. A natural killer−dendritic cell axis defines checkpoint therapy−responsive tumor microenvironments. *Nat Med* 2018;**24**:1178−91.
14. Super M, Doherty EJ, Cartwright MJ, Seiler BT, Langellotto F, Dimitrakakis N, et al. Biomaterial vaccines capturing pathogen-associated molecular patterns protect against bacterial infections and septic shock. *Nat Biomed Eng* 2022;**6**:8−18.
15. Wang H, Najibi AJ, Sobral MC, Seo BR, Lee JY, Wu D, et al. Biomaterial-based scaffold for *in situ* chemo-immunotherapy to treat poorly immunogenic tumors. *Nat Commun* 2020;**11**:1−14.
16. Ali OA, Huebsch N, Cao L, Dranoff G, Mooney DJ. Infection-mimicking materials to program dendritic cells *in situ*. *Nat Mater* 2009;**8**:151−8.
17. Zhang J, Chen C, Li A, Jing W, Sun P, Huang X, et al. Immunostimulant hydrogel for the inhibition of malignant glioma relapse post-resection. *Nat Nanotechnol* 2021;**16**:538−48.
18. Zhang X, Rao A, Sette P, Deibert C, Pomerantz A, Kim WJ, et al. IDH mutant gliomas escape natural killer cell immune surveillance by downregulation of NKG2D ligand expression. *Neuro Oncol* 2016;**18**:1402−12.
19. St-Amour I, Paré I, Alata W, Coulombe K, Ringuette-Goulet C, Drouin-Ouellet J, et al. Brain bioavailability of human intravenous immunoglobulin and its transport through the murine blood−brain barrier. *J Cerebr Blood Flow Metabol* 2013;**33**:1983−92.
20. Abbott NJ, Patabendige AA, Dolman DE, Yusof SR, Begley DJ. Structure and function of the blood−brain barrier. *Neurobiol Dis* 2010;**37**:13−25.
21. Terstappen GC, Meyer AH, Bell RD, Zhang W. Strategies for delivering therapeutics across the blood−brain barrier. *Nat Rev Drug Discov* 2021;**20**:362−83.
22. Su Y, Sohn S, Krown SE, Livingston PO, Wolchok JD, Quinn C, et al. Selective CD4+ lymphopenia in melanoma patients treated with temozolomide: a toxicity with therapeutic implications. *J Clin Oncol* 2004;**22**:610−6.
23. Sampson JH, Aldape KD, Archer GE, Coan A, Desjardins A, Friedman AH, et al. Greater chemotherapy-induced lymphopenia enhances tumor-specific immune responses that eliminate EGFRvIII-expressing tumor cells in patients with glioblastoma. *Neuro Oncol* 2011;**13**:324−33.
24. Lacroix M, Abi-Said D, Fourney DR, Gokaslan ZL, Shi W, DeMonte F, et al. A multivariate analysis of 416 patients with glioblastoma multiforme: prognosis, extent of resection, and survival. *J Neurosurg* 2001;**95**:190−8.
25. Chen C, Jing W, Chen Y, Wang G, Abdalla M, Gao L, et al. Intracavity generation of glioma stem cell−specific CAR macrophages primes locoregional immunity for postoperative glioblastoma therapy. *Sci Transl Med* 2022;**14**:eabn1128.
26. Min Y, Roche KC, Tian S, Eblan MJ, McKinnon KP, Caster JM, et al. Antigen-capturing nanoparticles improve the abscopal effect and cancer immunotherapy. *Nat Nanotechnol* 2017;**12**:877−82.
27. Chen S, Qiu Q, Wang D, She D, Yin B, Chai M, et al. Long acting carmustine loaded natural extracellular matrix hydrogel for inhibition of glioblastoma recurrence after tumor resection. *Front Chem Sci Eng* 2021:1−10.
28. Chen Q, Chen J, Yang Z, Xu J, Xu L, Liang C, et al. Nanoparticle-enhanced radiotherapy to trigger robust cancer immunotherapy. *Adv Mater* 2019;**31**:1802228.
29. Ali OA, Doherty E, Bell WJ, Fradet T, Hudak J, Laliberte MT, et al. The efficacy of intracranial PLG-based vaccines is dependent on direct implantation into brain tissue. *J Control Release* 2011;**154**:249−57.
30. Fehres CM, Bruijns SC, van Beelen AJ, Kalay H, Ambrosini M, Hooijberg E, et al. Topical rather than intradermal application of the TLR7 ligand imiquimod leads to human dermal dendritic cell maturation and $CD8^+$ T-cell cross-priming. *Eur J Immunol* 2014;**44**:2415−24.
31. Wang QT, Nie Y, Sun SN, Lin T, Han RJ, Jiang J, et al. Tumor-associated antigen-based personalized dendritic cell vaccine in solid tumor patients. *Cancer Immunol Immunother* 2020;**69**:1375−87.

32. Chen Q, Xu L, Liang C, Wang C, Peng R, Liu Z. Photothermal therapy with immune-adjuvant nanoparticles together with checkpoint blockade for effective cancer immunotherapy. *Nat Commun* 2016;**7**:1−13.
33. Obeid M, Tesniere A, Ghiringhelli F, Fimia GM, Apetoh L, Perfettini J-L, et al. Calreticulin exposure dictates the immunogenicity of cancer cell death. *Nat Med* 2007;**13**:54−61.
34. Kroemer G, Galluzzi L, Kepp O, Zitvogel L. Immunogenic cell death in cancer therapy. *Annu Rev Immunol* 2013;**31**:51−72.
35. Galluzzi L, Buqué A, Kepp O, Zitvogel L, Kroemer G. Immunogenic cell death in cancer and infectious disease. *Nat Rev Immunol* 2017;**17**: 97−111.
36. Lotze MT, Tracey KJ. High-mobility group box 1 protein (HMGB1): nuclear weapon in the immune arsenal. *Nat Rev Immunol* 2005;**5**: 331−42.
37. Yang Y, Nam GH, Kim GB, Kim YK, Kim IS. Intrinsic cancer vaccination. *Adv Drug Deliv Rev* 2019;**151**:2−22.
38. Chen DS, Mellman I. Oncology meets immunology: the cancer-immunity cycle. *Immunity* 2013;**39**:1−10.
39. Alifieris C, Trafalis DT. Glioblastoma multiforme: pathogenesis and treatment. *Pharmacol Ther* 2015;**152**:63−82.
40. Gajewski TF, Schreiber H, Fu YX. Innate and adaptive immune cells in the tumor microenvironment. *Nat Immunol* 2013;**14**:1014−22.
41. Filley AC, Henriquez M, Dey M. Recurrent glioma clinical trial, CheckMate-143: the game is not over yet. *Oncotarget* 2017;**8**:91779.
42. Sampson JH, Omuro AMP, Preusser M, Lim M, Butowski NA, Cloughesy TF, et al. A randomized, phase 3, open-label study of nivolumab versus temozolomide (TMZ) in combination with radiotherapy (RT) in adult patients (pts) with newly diagnosed, *O*-6-methylguanine DNA methyltransferase (MGMT)-unmethylated glioblastoma (GBM): CheckMate-498. *ASCO Meeting Abstracts*. 2016; **34**(15_suppl):TPS2079.
43. Palucka K, Banchereau J. Cancer immunotherapy *via* dendritic cells. *Nat Rev Cancer* 2012;**12**:265−77.
44. Gilboa E. DC-based cancer vaccines. *J Clin Invest* 2007;**117**: 1195−203.
45. Ardon H, De Vleeschouwer S, Van Calenbergh F, Claes L, Kramm CM, Rutkowski S, et al. Adjuvant dendritic cell-based tumour vaccination for children with malignant brain tumours. *Pediatr Blood Cancer* 2010;**54**:519−25.
46. Ardon H, Van Gool SW, Verschuere T, Maes W, Fieuws S, Sciot R, et al. Integration of autologous dendritic cell-based immunotherapy in the standard of care treatment for patients with newly diagnosed glioblastoma: results of the HGG-2006 phase I/II trial. *Cancer Immunol Immunother* 2012;**61**:2033−44.
47. Kleindienst P, Brocker T. Endogenous dendritic cells are required for amplification of T cell responses induced by dendritic cell vaccines *in vivo*. *J Immunol* 2003;**170**:2817−23.
48. Steinman RM, Banchereau J. Taking dendritic cells into medicine. *Nature* 2007;**449**:419−26.
49. Wang H, Mooney DJ. Biomaterial-assisted targeted modulation of immune cells in cancer treatment. *Nat Mater* 2018;**17**:761−72.
50. Wang H, Sobral MC, Zhang DK, Cartwright AN, Li AW, Dellacherie MO, et al. Metabolic labeling and targeted modulation of dendritic cells. *Nat Mater* 2020;**19**:1244−52.
51. Kim J, Li WA, Choi Y, Lewin SA, Verbeke CS, Dranoff G, et al. Injectable, spontaneously assembling, inorganic scaffolds modulate immune cells *in vivo* and increase vaccine efficacy. *Nat Biotechnol* 2015;**33**:64−72.
52. Shah NJ, Najibi AJ, Shih TY, Mao AS, Sharda A, Scadden DT, et al. A biomaterial-based vaccine eliciting durable tumour-specific responses against acute myeloid leukaemia. *Nat Biomed Eng* 2020;**4**:40−51.
53. Li AW, Sobral MC, Badrinath S, Choi Y, Graveline A, Stafford AG, et al. A facile approach to enhance antigen response for personalized cancer vaccination. *Nat Mater* 2018;**17**:528−34.
54. Bencherif SA, Warren Sands R, Ali OA, Li WA, Lewin SA, Braschler TM, et al. Injectable cryogel-based whole-cell cancer vaccines. *Nat Commun* 2015;**6**:1−13.
55. Zhao H, Lv X, Huang J, Huang S, Zhou H, Wang H, et al. Two-phase releasing immune-stimulating composite orchestrates protection against microbial infections. *Biomaterials* 2021;**277**:121106.
56. Chao Y, Liang C, Tao H, Du Y, Wu D, Dong Z, et al. Localized cocktail chemoimmunotherapy after *in situ* gelation to trigger robust systemic antitumor immune responses. *Sci Adv* 2020;**6**:eaaz4204.
57. Verbeke CS, Gordo S, Schubert DA, Lewin SA, Desai RM, Dobbins J, et al. Multicomponent injectable hydrogels for antigen-specific tolerogenic immune modulation. *Adv Healthc Mater* 2017;**6**:1600773.
58. Qiu Q, Li C, Yan X, Zhang H, Luo X, Gao X, et al. Photodynamic/photothermal therapy enhances neutrophil-mediated ibrutinib tumor delivery for potent tumor immunotherapy: more than one plus one?. *Biomaterials* 2021;**269**:120652.
59. Li F, Lai Y, Ye J, Saeed M, Dang Y, Zou Z, et al. Dual-targeting prodrug nanotheranostics for NIR-II fluorescence imaging-guided photo-immunotherapy of glioblastoma. *Acta Pharm Sin B* 2022;**12**: 3486−97.
60. Song X, Feng L, Liang C, Yang K, Liu Z. Ultrasound triggered tumor oxygenation with oxygen-shuttle nanoperfluorocarbon to overcome hypoxia-associated resistance in cancer therapies. *Nano Lett* 2016;**16**: 6145−53.
61. Phuengkham H, Song C, Yong TL. A Designer scaffold with immune nanoconverters for reverting immunosuppression and enhancing immune checkpoint blockade Therapy. *Adv Mater* 2019;**31**:1903242.
62. Mac Manus M, Lamborn K, Khan W, Varghese A, Graef L, Knox S. Radiotherapy-associated neutropenia and thrombocytopenia: analysis of risk factors and development of a predictive model. *Blood* 1997;**89**: 2303−10.
63. Lu M, Qiu Q, Luo X, Liu X, Sun J, Wang C, et al. Phyto-phospholipid complexes (phytosomes): a novel strategy to improve the bioavailability of active constituents. *Asian J Pharm Sci* 2019;**14**:265−74.
64. Qiu Q, Li C, Song Y, Shi T, Luo X, Zhang H, et al. Targeted delivery of ibrutinib to tumor-associated macrophages by sialic acid-stearic acid conjugate modified nanocomplexes for cancer immunotherapy. *Acta Biomater* 2019;**92**:184−95.
65. Qiu Q, Lu M, Li C, Luo X, Liu X, Hu L, et al. Novel self-assembled ibrutinib-phospholipid complex for potently peroral delivery of poorly soluble drugs with pH-dependent solubility. *AAPS PharmSciTech* 2018;**19**:3571−83.
66. Li C, Qiu Q, Liu M, Liu X, Hu L, Luo X, et al. Sialic acid-conjugate modified liposomes targeting neutrophils for improved tumour therapy. *Biomater Sci* 2020;**8**:2189−201.
67. Li C, Qiu Q, Gao X, Yan X, Fan C, Luo X, et al. Sialic acid conjugate-modified liposomal platform modulates immunosuppressive tumor microenvironment in multiple ways for improved immune checkpoint blockade therapy. *J Control Release* 2021;**337**:393−406.
68. Chen Q, Wang C, Zhang X, Chen G, Hu Q, Li H, et al. *In situ* sprayed bioresponsive immunotherapeutic gel for post-surgical cancer treatment. *Nat Nanotechnol* 2019;**14**:89−97.
69. Li P, Luo Z, Liu P, Gao N, Zhang Y, Pan H, et al. Bioreducible alginate-poly (ethylenimine) nanogels as an antigen-delivery system robustly enhance vaccine-elicited humoral and cellular immune responses. *J Control Release* 2013;**168**:271−9.
70. Kim SY, Noh YW, Kang TH, Kim JE, Kim S, Um SH, et al. Synthetic vaccine nanoparticles target to lymph node triggering enhanced innate and adaptive antitumor immunity. *Biomaterials* 2017;**130**:56−66.
71. Xu Y, Xiong J, Sun X, Gao H. Targeted nanomedicines remodeling immunosuppressive tumor microenvironment for enhanced cancer immunotherapy. *Acta Pharm Sin B* 2022;**12**:4327−47.
72. Wong CK, Cheung PF, Ip WK, Lam CW. Intracellular signaling mechanisms regulating toll-like receptor-mediated activation of eosinophils. *Am J Respir Cell Mol Biol* 2007;**37**:85−96.
73. Conniot J, Scomparin A, Peres C, Yeini E, Pozzi S, Matos AI, et al. Immunization with mannosylated nanovaccines and inhibition of the immune-suppressing microenvironment sensitizes melanoma to immune checkpoint modulators. *Nat Nanotechnol* 2019;**14**: 891−901.